Localized Topological States in Finite Non-Hermitian Photonic Lattices

Xiong Fan[1,2*], Wenchi Zang[1,2], Ming Ma[1,2*], Li-Gang Wang[3,4], and Tianxing Ma[5,6]

[1]*College of Electronic Science and Technology, National University of Defense Technology, Changsha 410073, China*
[2]*National Key Laboratory for Positioning, Navigation and Timing Technology, Changsha 410073, China*
[3]*School of Physics, Zhejiang University, Hangzhou 310058, China*
[4]*Zhejiang Key Laboratory of Micro-nano Quantum Chips and Quantum Control, Zhejiang University, Hangzhou 310058, China*
[5]*School of Physics and Astronomy, Beijing Normal University, Beijing 100875, China*
[6]*Key Laboratory of Multiscale Spin Physics (Ministry of Education), Beijing Normal University, Beijing 100875, China*

(Received 16 October 2025; accepted manuscript online 27 February 2026)

Edge states hybridize in finite-size topological materials, opening a gap between edge states which weakens the topological protection. Recent studies discover the recovery of zero modes in the finite-size non-Hermitian Su–Schrieffer–Heeger photonic lattices, which is of significance for fault-tolerant photonic integrations. In this paper, we reveal that the underlying mechanism is level attraction, a phenomenon common in non-Hermitian systems. To present that the level-attraction mechanism is generic for finite topological photonic lattices, we apply biased non-Hermitian potentials on the two-dimensional Qi–Wu–Zhang model and a second-order Bernevig–Hughes–Zhang model based on the spatial distribution of edge states, and demonstrate the evolution of edge states as the potential strength changes. The condition of decoupling the hybridized edge states is that the ratio between hybridization strength and biased non-Hermitian potential strength approaches zero; otherwise, the edge states remain coupled if non-Hermitian potential is small even when the zero real energy is recovered. The results show that the level-attraction mechanism recovers localized zero modes in all these finite-size topological models, and disorder only causes distribution fluctuations of localized edge states. Therefore, in the finite-size regime, zero modes are enhanced or protected by the level-attraction mechanism, offering a strategy for designing compact topological photonic devices.

DOI: 10.1088/0256-307X/43/4/040701 CSTR: 32039.14.0256-307X.43.4.040701

1. Introduction. Level repulsion, manifested as the anticrossing between coupled energy levels, constitutes a fundamental quantum phenomenon. In atomic systems, interacting energy levels repel to avoid degeneracy, while in periodic lattices, this repulsion governs band structure formation and gap emergence.[1] Conversely, level attraction, characterized by level coalescence, has recently gained prominence in hybrid quantum systems through diverse physical mechanisms.[2–12] For instance, phase-engineered coupling achieves tunable anticrossing gaps by precisely controlling relative phase shifts between driving fields, enabling phase-locked synchronization;[5,8] dissipative coupling, mediated by the cavity Lenz effect[6] or shared dissipation channels,[7] likewise induces level coalescence. Given that level repulsion underlies a wide range of phenomena in physics and quantum chemistry,[1,4] its counterpart, level attraction, is anticipated to describe a variety of new physical effects. Level attraction always generates exceptional points,[13] facilitating many applications such as topological energy transfer,[14] quantum metrology and sensing,[15–19] and cloaking.[20–23] Further, the recent observation of energy-band attraction in Mie resonators has provided an accessible platform for studying non-Hermitian photonic band structures.[24] Despite these advances, level attraction in topological materials still remains largely unexplored and presents opportunities to harness its unique properties for robust quantum technologies.

A recent study on non-Hermiticity enhanced topological protection of edge states also demonstrates the level-attraction phenomenon in finite-size systems.[25] Finite-size topological models open a finite gap between edge states due to hybridization of edge modes, which means the reduction of topological protection, and non-Hermitian potentials make the real energies of edge states converge. According to calculations on a quantum spin Hall effect (QSHE) model and the Su–Schrieffer–Heeger (SSH) model, the gaps decrease exponentially with increasing system size.[26,27] Therefore, the gaps are negligible in the thermodynamic limit. In the perspective of applications, miniaturized devices are preferable. Stimulated by the development of non-Hermitian Hamiltonian with parity-time (PT) symmetry,[28] an optical lattice experiment of the SSH model discovered that the gap can be closed and zero modes are recovered by adding PT-symmetric non-Hermitian potentials.[25] The pioneering work of Ref. [25]

*Corresponding authors. Email: fanxiong24@nudt.edu.cn; maming@nudt.edu.cn
© 2026 Chinese Physical Society and IOP Publishing Ltd. All rights, including for text and data mining, AI training, and similar technologies, are reserved.

experimentally demonstrates the phenomenon of the recovery of topological zero modes in SSH lattices; however, the underlying physical mechanism governing this recovery remains incompletely explored. In this paper, we construct an effective Hamiltonian for edge states to explain and generalize this phenomenon. Furthermore, we provide a quantitative criterion and physical intuition for edge-state dehybridization and investigate the robustness of this phenomenon against disorder, thereby establishing a theoretical framework for this phenomenon.

Topological photonics has emerged as a revolutionary paradigm for controlling light propagation by leveraging concepts from topological condensed matter physics.[29] Initial breakthroughs demonstrate photonic analogs of the integer quantum Hall effect using magneto-optical materials to break time-reversal symmetry and achieve unidirectional edge states protected against backscattering.[30–33] Subsequent research establishes time-reversal-invariant systems exhibiting photonic QSHEs through pseudospin engineering in bianisotropic metamaterials[34,35] and valley-Hall effects via inversion symmetry-broken hexagonal photonic crystals.[36–39] The field has since expanded to include higher-order topological insulators hosting lower-dimensional boundary states, such as the observation of robust corner states in C_{6v}-symmetric photonic crystals realizing a higher-order QSHE.[40] Non-Hermitian topological phases have also been explored, such as the topology induced solely by system non-Hermicity[41,42] and topology independent of non-Hermicity.[43] Recent advances encompass 3D topological phenomena, including Weyl points,[44] synthetic dimensions,[45] and topological lasers that exploit protected edge modes for disorder-resistant purpose.[46,47] These developments establish topological photonics as a versatile framework for controlling light with unprecedented robustness, enabling applications in topological circuit,[48,49] quantum light manipulation,[50] and next-generation photonic devices immune to fabrication imperfections.

In this Letter, we establish effective Hamiltonians for edge states and identify level attraction induced by non-Hermiticity as the mechanism underlying the recovery of zero modes in the photonic SSH model. Finite-size lattices lead to coupling between edge states, and the biased PT-symmetric potentials decouple them. The former causes the edge-state energies repel each other, whereas the latter causes the real parts of the edge-state energies to converge and opens a gap in the imaginary part. Further, we go beyond the one-dimensional SSH model by demonstrating that this mechanism is generically applicable to higher-dimensional and higher-order topological photonic lattices. Below, we examine the Qi–Wu–Zhang (QWZ) model of quantum anomalous Hall effect (QAHE)[51] and a second-order Bernevig–Hughes–Zhang (BHZ) model.[52,53] By applying imaginary potentials to both models according to their symmetries,we observe the recovery of zero modes and localized edge states. Regarding other topological models, level attraction can be realized by applying imaginary potentials based on their symmetries.

2. Finite-Size SSH Model. A typical model we study is the SSH model with PT-symmetric on-site potentials $\gamma_z = \mathrm{i}\nu$,[25]

$$H_{\mathrm{SSH}} = \left(t_1 \sum_{j=1}^{N} |j,B\rangle\langle j,A| + t_2 \sum_{j=1}^{N-1} |j+1,A\rangle\langle j,B| + \mathrm{h.c.} \right) + \gamma_z \sum_{j=1}^{N} (|j,A\rangle\langle j,A| - |j,B\rangle\langle j,B|), \tag{1}$$

where $|j,A,$ or $B\rangle$ is the real-space state, and j denotes the unite cell, one of which includes two sublattices. t_1 and t_2 are the intracell and intercell couplings, respectively, and ν describes the gain or loss strength. When $\gamma_z = 0$, the Hermitian SSH model is topologically nontrivial if $t_2 > t_1 \geq 0$, and the bulk-band gap equals $2(t_2 - t_1)$ under periodic boundary condition.[54]

To analyze the character of edge states under PT-symmetric on-site potentials, we derive the non-Hermitian low-energy approximation Hamiltonian. For the Hermitian case ($\nu = 0$), following the recursive method in Ref. [27], the energy of the edge states is expressed as

$$E_{\pm} \simeq \pm \frac{t_2^2 - t_1^2}{t_2} \left(\frac{t_1}{t_2}\right)^N = \pm \frac{t_2^2 - t_1^2}{t_2} \exp\left(-N/\xi\right), \tag{2}$$

where N is the number of unit cells, $\xi = -\ln^{-1}(t_1/t_2)$ is the localization length of corresponding wave functions. The larger the bulk-band gap is, the shorter the localization length becomes. For an infinite-size system, the left and right edge states are separate zero modes with the wave functions $|\psi_{\mathrm{Left(L)}}\rangle = (1/l_{\mathrm{SSH}}) \sum_j (-t_1/t_2)^{j-1} |j,A\rangle$ and $|\psi_{\mathrm{Right(R)}}\rangle = (1/l_{\mathrm{SSH}}) \sum_j (-t_1/t_2)^{N-j} |j,B\rangle$, with the normalization constant $l_{\mathrm{SSH}} = \sqrt{t_2^2/(t_2^2 - t_1^2)}$, and each state is located on the A or B sublattice. For a finite-size system, the edge states have energies near zero given by Eq. (2), and their wave functions are $\psi_{\pm} = (1/\sqrt{2})(\psi_{\mathrm{L}} \pm \psi_{\mathrm{R}})$. Equation (2) can be considered the result of coupling between two states originally localized at the left and right boundaries, respectively. Since the edge states lie within the bulk-band gap, coupling between the edge states and the bulk states is negligible. Consequently, the low-energy approximation applies, and the two-level system provides a complete description of the edge modes. The effective coupling can be calculated after the above analysis by treating the finite-size Hamiltonian as a perturbation,

$$t_{\mathrm{eff}} = \langle \psi_{\mathrm{L}} | H | \psi_{\mathrm{R}} \rangle \simeq (-1)^{N+1} \frac{t_2^2 - t_1^2}{t_2} \exp\left(-N/\xi\right). \tag{3}$$

Then, we add the PT-symmetric on-site potentials $\gamma_z = \mathrm{i}\nu$. The effective non-Hermitian two-level system is described by

$$H_{\mathrm{eff}} = t_{\mathrm{eff}} \sigma_x + \gamma_z \sigma_z \tag{4}$$

with the eigenvalues $E_{\pm} = \pm\sqrt{t_{\mathrm{eff}}^2 - \nu^2}$. As ν increases, i.e., as the gain or loss strength grows, the energies $E_{\pm}$ converge to zero real part when the on-site imaginary potential passes through the exceptional point; moreover, these states acquire imaginary energy, indicating growing or dissipating modes. This phenomenon is

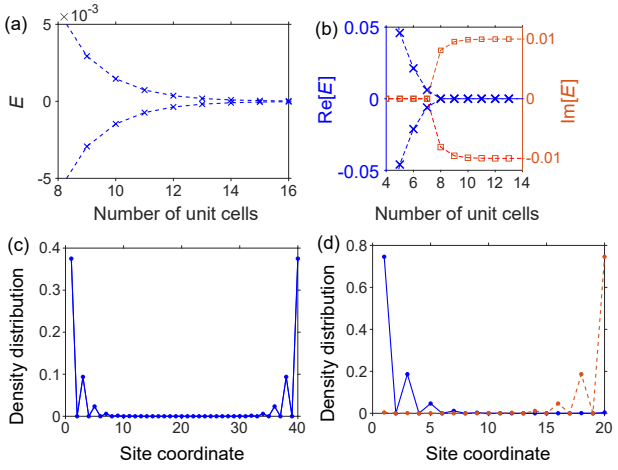

Fig. 1. Energy of states near zero versus system size for (a) $\nu = 0$ and (b) $\nu = 0.01$. Other parameters are $t_1 = 1$ and $t_2 = 2$. The cross markers "×" and square markers "□" denote the numerically computed real and imaginary parts of the energy, respectively; the dashed lines are obtained from Eq. (4). Density distribution: (c) for a system of 20 unit cells with $\nu = 0$, and (d) for a system of 10 unit cells with $\nu = 0.01$.

called level attraction. In Fig. 1(a), the comparison between the numerical results and Eq. (4) shows that the equation effectively describes the behavior of eigenvalues near zero energy. As shown in Fig. 1(b), for a system with $\nu = 0.01$, the real part of the energy vanishes at a finite size due to level attraction induced by non-Hermitian potentials; additionally, these states acquire a growing or dissipative factor. Figure 1(b) demonstrates exceptional-point behavior in discrete parameter space, observed when the system size is around 7 unit cells. As ν increases, the exceptional point shifts to smaller system sizes. In contrast, a small gap always exists in a finite-size Hermitian system with $\nu = 0$ [Fig. 1(a)]. Furthermore, the density distributions of the edge states vividly illustrate the impact of non-Hermiticity. Figure 1(c) demonstrates the hybridized nature of the edge state in the Hermitian system ($\nu = 0$), where the probability density is distributed across both boundaries. In contrast, upon introducing a non-Hermitian potential ($\nu = 0.01$), the state becomes strongly localized at one boundary—even in a system half the size—as depicted in Fig. 1(d).

Now we show that level attraction protects zero modes from disorders in the SSH models with PT-symmetric potentials. The disorder is set as

$$\Delta t_j = \kappa R_j, \tag{5}$$

where κ is the disorder strength, and $R_j \in (-0.5, 0.5)$. Then each coupling bond $t_j \to t_j + \Delta t_j$, which preserves the underlying chiral symmetry. In Fig. 2(a), we show the energy of edge states versus the gain or loss strength in two disordered systems with the disorder strength $\kappa = 0.25$. Theoretical results are obtained by adopting the edge energy t_{eff} from the $\nu = 0$ case. Comparing the theoretical with numerical results, the non-Hermitian two-level Hamiltonian perfectly describes the two edge states. Both disordered cases demonstrate the recovery of zero-real-part

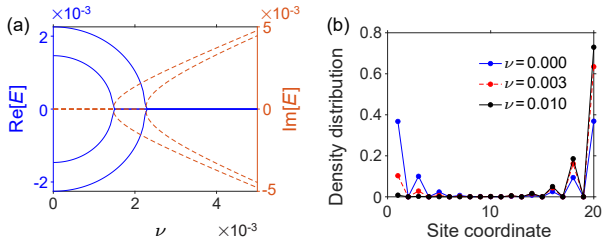

Fig. 2. (a) Energy of states near zero versus ν for two disorder configuratons; and (b) density distribution of an edge state versus site coordinate. The number of unit cells is 10, i.e., the number of sites is 20, $t_1 = 1$ and $t_2 = 2$. The disorder strength is fixed as $\kappa = 0.25$. Theoretical and numerical results coincide.

energy states when the on-site imaginary potential passes through the exceptional point, and these states acquire growing or dissipating factors. Disorder causes fluctuations in t_{eff} and may reduce the localization of the edge states. In Fig. 2(b), we show the density distribution of a finite-size SSH model with the disorder strength $\kappa = 0.25$. As shown, the density distribution shifts to one boundary when ν is increased from 0 to 0.01. The phase diagram of hybridized and localized states in the (κ, ν) parameter space is provided in the Supplementary Materials (SM). It further shows that t_{eff} exhibts only slight variation under moderate disorder. Thus, in the presence of sufficiently strong non-Hermitian potentials, level attraction not only recovers zero real energy in the non-Hermitian SSH model but also enhances topological protection in the presence of disorder.

The alternative method of realizing zero modes is increasing the number of unit cells. We note that two methods of realizing zero modes differ fundamentally. From Eq. (3), enlarging the system size realizes zero modes by reducing the effective coupling between the edge states. In contrast, applying PT-symmetric potentials does not alter the effective coupling coefficient in Eq. (3), indicating that the edge states remain coupled for small ν, even when zero real energy is recovered. Nevertheless, increasing ν localizes the edge states at one boundary. The reason is as follows. The gap between biased on-site potentials is $\Delta E = 2i\nu$, which, under the infinite-system approximation, is also the energy gap between the two isolated edge states. According to perturbation theory, current wave functions $\psi'_{\text{L/R}}$ satisfy $\psi'_{\text{L/R}} - \psi_{\text{L/R}} \sim \frac{t_{\text{eff}}}{\Delta E}\psi_{\text{R/L}}$ for a finite-size model. As a result, the edge states become localized at a single boundary when $t_{\text{eff}}/\Delta E \sim 0$. Physically, the suppression of edge-state hybridization by gain and loss can be understood through an analogy with two coupled classical oscillators (see SM). In addition, the above discussion enables us to explain certain results in Ref. [55] from our perspective. For instance, the decrease in the real energy gap with increasing gain/loss strength becomes slower when the imaginary potential is applied to a smaller portion of the edge-state distribution. The weaker dependence reflects a reduction in level attraction.

To demonstrate the generality of the level-attraction mechanism beyond one-dimensional systems, we next investigate photonic zero modes in the QWZ model and in

a second-order BHZ models. The QWZ and BHZ models are typical, as they effectively capture the QAHE and the QSHE, respectively. Since the BHZ model is the time-reversal-invariant counterpart of the QWZ model, discussing both models is unnecessary in the context of this paper. However, the second-order BHZ model is worth verifying, as it provides additional degrees of freedom for applications in integrated topological devices.[40]

3. Finite-Size QWZ Model. The finite-size QWZ model opens a gap in the edge-state dispersion, rendering the edge states unstable under disorder.[26] As shown below, non-Hermitian potentials close this gap and thereby protect the edge states against disorder.

First we analyze the low-energy behavior of the QWZ model. The QWZ model in momentum space is[54]

$$H_{\mathrm{QWZ}} = t_1 \sin k_x \sigma_x + t_2 \sin k_y \sigma_y + (M + t_1 \cos k_x + t_2 \cos k_y)\sigma_z, \tag{6}$$

where the Pauli matrices $\sigma_{x,y,z}$ are the orbital operators, M is the staggered on-site potential depending on the two internal freedoms, t_1 and t_2 are hopping parameters in the x and y directions, respectively, and we set $t_1 = t_2 = 1$. The topology of the band structure is nontrivial if $M \in (-2, 0) \cup (0, 2)$.[54] The bulk gap in Eq. (6) equals $2(M + 2)$ if $M \in (-2, -1)$, and we write this relationship as $\Delta_{\mathrm{B}} = 2(M + 2)$. Considering the open boundary condition in the y direction and periodic boundary condition in the x direction, the Hamiltonian becomes

$$H_{\mathrm{QWZ}}(k_x) = \left[\sum_{j=1}^{N_y - 1} |j+1\rangle\langle j| \otimes (\sigma_z + \mathrm{i}\sigma_y)/2 + \mathrm{h.c.} \right] + \sum_{j=1}^{N_y} |j\rangle\langle j| \otimes (\cos k_x \sigma_z + \sin k_x \sigma_x + M\sigma_z). \tag{7}$$

Without loss of generality, assume $M \in (-2, -1)$, and define $\delta = -1 - M$, i.e., $\delta = 1 - \Delta_{\mathrm{B}}/2$ and $\delta \in (0, 1)$. In the thermodynamic limit $N_y \to \infty$, the gap of edge states closes at $k_x = 0$, and the edge states at $k_x = 0$ are caculated as $|\psi_{\mathrm{L}}\rangle = (1/l_{\mathrm{QWZ}}) \sum_j \delta^{j-1} |j, \alpha\rangle - \delta^{j-1} |j, \beta\rangle$ and $|\psi_{\mathrm{R}}\rangle = (1/l_{\mathrm{QWZ}}) \sum_j \delta^{N_y - j} |j, \alpha\rangle + \delta^{N_y - j} |j, \beta\rangle$ with the orbitals α and β. $l_{\mathrm{QWZ}} = \sqrt{2/(1 - \delta^2)}$ is the normalization constant. The two edge states at $k_x = 0$ are degenerate in momentum space but spatially separated at the two boundaries slong the y direction. The localization length is $\xi = -\ln^{-1} \delta$, which increases as the bulk gap Δ_{B} shrinks. For a finite size in the y direction, the edge states hybridize, similar to the case in the SSH model, thereby opening a gap between them. We now calculate the edge-state energy for finite-size systems. Since k_x is a good quantum number and Δ_{B} is finite, only the two edge states at $k_x = 0$ need be considered within the low-energy approximation. By calculating the coupling strength $t_{\mathrm{eff}} = \langle \psi_{\mathrm{L}} | H | \psi_{\mathrm{R}} \rangle$, the energies of the two edge states are $E_{\pm} = \pm t_{\mathrm{eff}} \simeq \mp (1 - \delta^2) \exp(-N_y/\xi)$.

We then use non-Hermitian potentials to recover zero modes and edge states in the finite-size QWZ model.

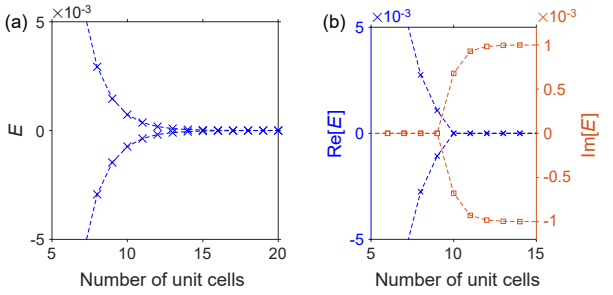

Fig. 3. Energy of states near zero versus N_y at $k_x = 0$ for (a) $\gamma_z = 0$ and (b) $\gamma_z = 0.001\mathrm{i}$, with $M = -1.5$. The cross markers "×" and square markers "□" denote the numerically computed real and imaginary parts of the energy, respectively; the dashed lines are obtained from Eq. (4). ν is set as zero at the central site when N_y is odd.

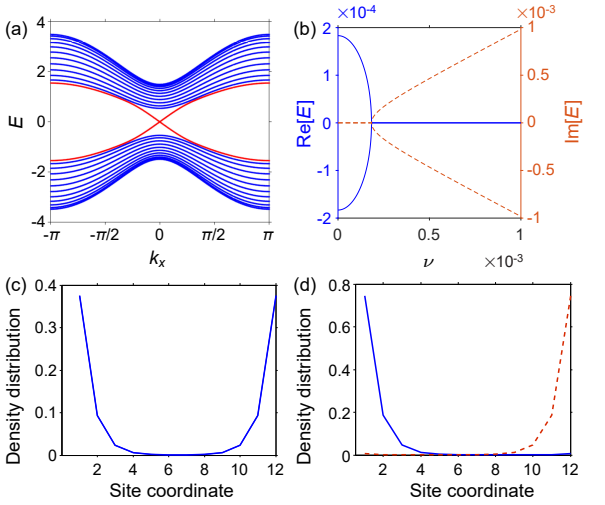

Fig. 4. Energy–momentum dispersion of the QWZ model for (a) $\gamma_z = 0$; and (b) edge-state energies versus ν. Density distributions corresponding to (c) the near-zero-energy states and (d) the zero mode with $\nu = 0.001$. The number of unit cells in the y direction is 12 and $M = -1.5$.

Without loss of generality, we assume that N_y is even. To close the gap, we apply imaginary potentials with opposite signs on the two sides along the y direction, as follows:

$$V = \gamma_z \sigma_z \otimes I_{N_y/2 \times N_y/2}, \tag{8}$$

which means applying potentials γ_z to the lower half of the sites, from 1 to $N_y/2$ in the y direction, and $-\gamma_z$ to the upper half, from $N_y/2 + 1$ to N_y. Now, each pair of edge states at a given k_x satisfies Eq. (4). In Figs. 3(a) and 3(b), we show the edge-state energy versus the number of unit cells at $k_x = 0$, for $\gamma_z = 0$ and $\gamma_z = 0.001\mathrm{i}$, respectively. Compared with Fig. 3(a), figure 3(b) achieves zero real energy at a smaller size and exhibits exceptional-point behavior. The theoretical results show excellent agreement with the numerical simulations shown in Fig. 3.

To examine the dispersion and edge states, figures 4(a) and 4(c) show the energy spectrum and a hybridized state near zero, respectively, for $\gamma_z = 0$; figures 4(b) and 4(d) display the energy versus ν and two zero modes, respectively, for $\gamma_z = 0.001\mathrm{i}$. Figure 4(c) is the consequence of coupling of two edge states originally localized at either boundary like the chiral states in Fig. 4(d).

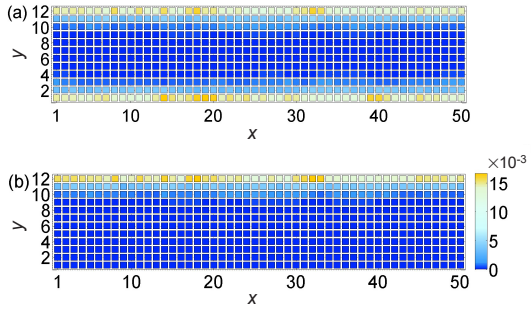

Fig. 5. Density distribution of the edge states in the stripe for (a) $\nu = 0$ and (b) $\nu = 0.001$. $M = -1.5$ and $\kappa = 0.25$. The number of unit cells is 12 along the y direction with open boundary condition and 50 in the x direction with periodic boundary condition.

Figure 4(b) demonstrates the level-attraction phenomenon and the exceptional point in the QWZ model. Moreover, from Fig. 4(b), we deduce a coupling strength of $\sim 2\times 10^{-4}$ from the $\nu = 0$ case. Thus, according to the discussion in the previous section, $\gamma_z = 0.001\mathrm{i}$ in Fig. 4(d) is large enough to recover the zero-real-energy mode and decouple the two edge states.

To study the effect of disorders, we use the real-space Hamiltonian of a stripe with periodic boundary conditions along the x direction,

$$H_{\mathrm{QWZ}} = \Bigg[\sum_{j_x=1}^{N_x}\sum_{j_y=1}^{N_y} t_{1j}|j_x+1,j_y\rangle\langle j_x,j_y|\otimes(\sigma_z+\mathrm{i}\sigma_x)/2 + \mathrm{h.c.}\Bigg] + \Bigg[\sum_{j_x=1}^{N_x}\sum_{j_y=1}^{N_y-1} t_{2j}|j_x,j_y+1\rangle\langle j_x,j_y|\otimes(\sigma_z+\mathrm{i}\sigma_y)/2 + \mathrm{h.c.}\Bigg] + M\sum_{j_x=1}^{N_x}\sum_{j_y=1}^{N_y}|j_x,j_y\rangle\langle j_x,j_y|\otimes\sigma_z, \tag{9}$$

where $t_{1j} = t_1 + \kappa R_{1j}$ and $t_{2j} = t_2 + \kappa R_{2j}$. κ is the disorder strength, and $R_{1j,2j} \in (-0.5, 0.5)$. In Fig. 5, we set the disorder strength to $\kappa = 0.25$ and consider a stripe with periodic boundary conditions in the x direction to simulate an infinitely long sample. When the non-Hermitian potential is absent, the edge states at the two boundaries along the y direction are coupled as shown in Fig. 5(a). Compared with the clean case, disorder induces fluctuations in the density distribution along the x direction. In contrast, in Fig. 5(b), we apply a non-Hermitian potential with $\nu = 0.001$ to the stripe, localizing the edge state at one boundary. The phase diagram in the (κ, ν) space clearly demonstrates that the non-Hermitian potential separates the hybridized phase from the localized phase (see SM). Therefore, the non-Hermitian potential continues to suppress edge-state hybridization across the two boundaries even in the presence of disorder, while disorder primarily causes fluctuations in the density distrituion.

4. Finite-Size Second-Order BHZ Model. We now demonstrate that the level-attraction phenomenon exists in the second-order BHZ model as well. First we introduce the essential features of its Hamiltonian. The second-order BHZ model hosts corner states, localized at the four corners of a rectangular or square system, whereas the first-order BHZ model supports helical edge states. The Hamiltonian is[52,53]

$$\begin{aligned} H_{\mathrm{BHZ}}(k_x,k_y) = {} & [M + t_0(\cos k_x + \cos k_y)]\tau_z\otimes\sigma_0 \\ & + \Delta_1(\sin k_x\tau_x\otimes\sigma_x + \sin k_y\tau_x\otimes\sigma_y) \\ & + \Delta_2(\cos k_x - \cos k_y)\tau_y\otimes\sigma_0, \end{aligned} \tag{10}$$

in which τ and σ are Pauli matrices describing orbitals and spins, respectively, M is the staggered on-site real potential depending on the two orbital freedoms, t_0 is the orbital-dependent hopping parameter, τ_0 and σ_0 are 2×2 identity matrices, Δ_1 represents the spin-orbit coupling, the Δ_2 term describes the orbital current. We set $t_0 = 1$ and $\Delta_1 = 1$. Equation (10) mixes orbitals and spins, thus exhibits the QSHE with conserved pseudo-spins if $\Delta_2 = 0$. When $\Delta_2 \neq 0$, the Chern number is zero because Δ_2 opens a gap in the edge-state dispersion; however, the diagonal winding number along $k_x = \pm k_y$ is nontrivial, indicating that Eq. (10) describes a second-order topological insulator.[53] The bulk gap in Eq. (10) equals $2(M+2)$ for $M \in (-2,-1)$. Under open boundary conditions along the y direction, with $M \sim -1$ and $\Delta_2 \sim 0$, the edge-state spectrum approximates $E^{\mathrm{e}}_{k_x} \simeq \pm\sqrt{k_x^2 + \Delta_2^2 + \delta^2}$ with $\delta = -1 - M$. Assuming $M \sim -1$ and $\Delta_2 \neq 0$, the edge-state gap opens, and the corner states become localized near the four corners.

We provide the analytical wave functions of these corner states after some algebras. Applying the open boundary condition in the x and y directions, we have

$$\begin{aligned} H_{\mathrm{BHZ}} = \sum_{\langle j,j'\rangle,s=\uparrow,\downarrow}\Bigg[& \frac{M}{2}(|j,d,s\rangle\langle j,d,s| - |j,f,s\rangle\langle j,f,s|) \\ & + \frac{t_0}{2}(|j,d,s\rangle\langle j',d,s| - |j,f,s\rangle\langle j',f,s|) \\ & + \frac{\Delta_1}{2}\eta_{jj's\bar{s}}(|j,d,s\rangle\langle j',f,\bar{s}| + |j,f,s\rangle\langle j',d,\bar{s}|) \\ & + \mathrm{i}\frac{\Delta_2}{2}\xi_{jj'}(|j,d,s\rangle\langle j',f,s| - |j,f,s\rangle\langle j',d,s|) + \mathrm{h.c.}\Bigg], \end{aligned} \tag{11}$$

where d and f are orbitals, and

$$(\eta_{jj's\bar{s}}, \xi_{jj'}) = \begin{cases} (\mathrm{i}, 1), & x \text{ direction}, \ s\bar{s} = \uparrow\downarrow, \downarrow\uparrow; \\ (1, -1), & y \text{ direction}, \ s\bar{s} = \uparrow\downarrow; \\ (-1, -1), & x \text{ direction}, \ s\bar{s} = \downarrow\uparrow. \end{cases}$$

By listing the system of linear equations, the zero-energy corner state centered at $(1,1)$ is solved as $|\psi_{1,1}\rangle \simeq (1/l)\sum_{j,\tau,s} c_{j,\tau,s}c_{\tau,s}|j,\tau,s\rangle$ with $c_{\tau,s}$ the phase factor, $c_{j,\tau,s}$ the decay coefficient, and l the normalization coefficient. Wave functions at other corners have similar forms: the decay coefficient remains unchanged, and the phase factor is modified accordingly (see the SM). In finite-size systems, these corner states hybridize primarily at the boundary, because the band gaps of the bulk and edge states are much larger than that of the corner states. The energy levels and density distribution of a state near zero energy are shown in Figs. 6(a) and 6(c), respectively. The phases "I", "II", and "III" denote the bulk states,

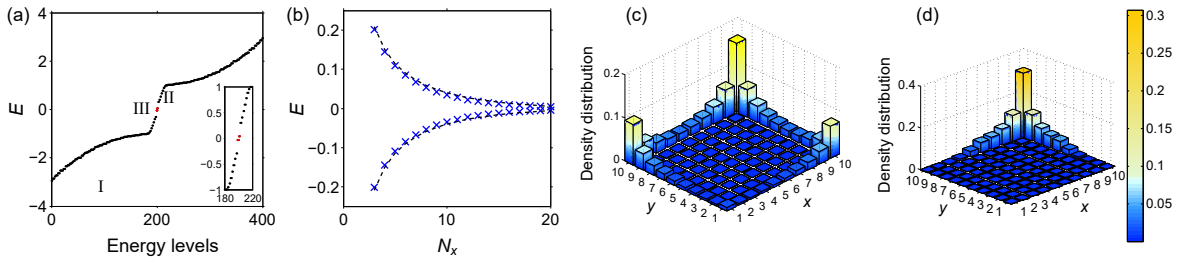

Fig. 6. (a) Energy spectra. "I", "II", and "III" phases denote the bulk states, edge states, and corner states, respectively. The inset clearly shows the finite energy gap between the corner states. (b) Energy of states near zero energy in square systems versus N_x, where the cross markers represent numerical results and the dashed line shows the theoretical estimations. (c) Density distribution of a state near zero energy with $\gamma_z = 0$. (d) Density distribution of a corner state with $\gamma_z = 0.3$i. The number of unit cells in the x and y directions is 10 for (a), (c), and (d). Parameters are set as $\Delta_2 = 0.2$ and $M = -1$.

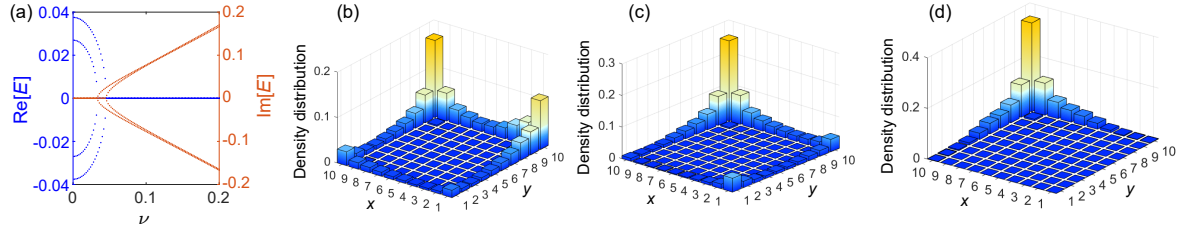

Fig. 7. (a) Energy of the corner states versus ν for a disorder strength of $\kappa = 0.25$. Density distributions of a corner state with (b) $\nu = 0$, (c) $\nu = 0.05$, and (d) $\nu = 0.2$. Other parameters are identical to those in Fig. 6.

edge states, and corner states, respectively. Corner states hybridize with nearest neighboring corner states to form a "triangle state", as shown in Fig. 6(c), thereby opening a finite energy gap of ∼0.08 in phase "III".

With the corner-state wave functions, the low-energy behavior of the corner states is accessible. To realize biased imaginary potentials between different corner states, two blocks at the diagonal direction must be subjected to the same potential, while two adjacent blocks take opposite potentials. Therefore, we set the piecewise potentials as

$$V(j_x, j_y) = \begin{cases} \gamma_z, & \{j_x \in [0, N_x/2], j_y \in [0, N_y/2]\}; \\ \gamma_z, & \{j_{x(y)} \in [N_{x(y)}/2+1, N_{x(y)}]\}; \\ -\gamma_z, & \{j_x \in [0, N_x/2], j_y \in [N_y/2+1, N_y]\}; \\ -\gamma_z, & \{j_x \in [N_x/2+1, N_x], j_y \in [0, N_y/2]\}, \end{cases} \tag{12}$$

in which j_x and j_y are the x and y coordinates, respectively, and N_x and N_y represent the number of unit cells. Taking $|\psi_{1,1}\rangle$, $|\psi_{N_x,N_y}\rangle$, $|\psi_{N_x,1}\rangle$, and $|\psi_{1,N_y}\rangle$ as bases, the non-Hermitian Hamiltonian matrix of the corner states approximates

$$H_{\text{corner}} \simeq \begin{pmatrix} \gamma_z & 0 & t_x & t_y \\ 0 & \gamma_z & t_y & t_x \\ t_x^* & t_y^* & -\gamma_z & 0 \\ t_y^* & t_x^* & 0 & -\gamma_z \end{pmatrix}, \tag{13}$$

where

$$t_x = \langle \psi(1,1) | H_{\text{BHZ}} | \psi(N_x, 1) \rangle,$$

and

$$t_y = \langle \psi(1,1) | H_{\text{BHZ}} | \psi(1, N_y) \rangle$$

(see SM). t_x and t_y describe the coupling strength of corner states in the x and y directions, respectively. The corresponding coupling strength decreases as N_x or N_y increases. H_{corner} respects the C_2 symmetry of the system, and the eigenvalues are $E = \pm\sqrt{t_x t_x^* + t_y t_y^* + \gamma_z^2}$, doubly degenerate. From Eq. (13), a two-horn-like state may appear if either t_x or t_y is much weaker than the other—a condition realizable in a rectangular sample. Figure 6(a) shows the energy levels of bulk, edge, and corner states; the inset shows the finite gap between the two pairs of corner states. The theoretical estimations of near-zero-energy states are plotted in Fig. 6(b) for comparison with numerical results. The error is negligible, indicating that the Hamiltonian Eq. (13) provides an effective description for corner states. γ_z is 0.3i in Fig. 6(d), which is large enough to yield zero real energy and localize the corner states, consistent with the much smaller gap in Fig. 6(b). As shown in Fig. 6(d), the corner state near (10, 10) is localized, and the density distribution decays almost exponentially along the edges, as previously derived. Therefore, the non-Hermitian potential enhances the localization of corner states in the finite-size second-order BHZ model.

Regarding disorders in the second-order BHZ model, the conclusion is similar to that in the previous two models. We investigate disorder in the hopping parameters and set $t_{0j} = t_0 + \kappa R_{0j}$, $\Delta_{1j} = \Delta_1 + \kappa R_{1j}$, and $\Delta_{2j} = \Delta_2 + \kappa R_{2j}$, where $R_{0j,1j,2j} \in (-0.5, 0.5)$ and j denotes the bond index. For moderate-strength disorders, the density distribution of the corner states is disturbed, and non-Hermitian potentials localize the coupled corner state at fewer corners, since orinially the corner state may be distributed at all corners when disorder appears. For instance, figures 7(b)–7(d) show the density distribution of a corner state with hopping disorder strength $\kappa = 0.25$ for different values of ν. As ν increases from 0 to 0.05 and then to 0.2, the

corner state localizes progressively, shifting from four corners to three and finally to one. In Fig. 7(d), hybridization between different corner states is completely suppressed. The corresponding level-attraction dispersion is shown in Fig. 7(a). We observe that the zero real energy is recovered as ν increases, and the two-fold degeneracy is lifted by disorder. The SM provides the phase diagram of the hybridized phase and the localized phase, with the conclusion consistent with those of the previously discussed models (see SM for details).

5. Discussion and Conclusion. Photonic lattices provide an ideal platform for realizing non-Hermitian effects.[29] In photonics, amplification and absorption are more controllable than in solids. For instance, optical pumping[56] can be used to achieve photon gain, while loss is inherent in all photonic devices. Additionally, pseudospins and artificial orbitals can be constructed in photonic lattices using the angular momentum and different resonant modes of electromagnetic waves.[40,57] The level attraction of chiral edge states and corner states can be experimentally realized in two-dimensional arrays of ring resonators[58] and dielectric cylinders,[40] respectively. The principle presented in this paper is applicable to analogous systems, despite differences in their Hamiltonians. Extending the framework to three-dimensional topological photonic lattices with surface or hinge states,[44,52,59] we propose applying biased non-Hermitian potentials to the coupled edge states to control their hybridization. It is also worth noting that, although level attraction has been realized through diverse approaches, to the best of our knowledge, all current research on the topic remains confined to non-Hermitian systems. An open question is whether it can manifest in Hermitian systems, where the recovered zero modes in finite systems exhibit no imaginary splitting.

In summary, we have demonstrated that the level-attraction mechanism arising from non-Hermiticity is the origin of the recovery of localized zero modes in finite-size topological photonics lattices, and that the biased imaginary potentials induce the dehybridization of edge modes in real space. The condition for decoupling the hybridized edge states is that the ratio of the hybridization strength to the biased non-Hermitian potential strength approaches zero; otherwise the edge states remain coupled even when the zero real energy is recovered, provided the non-Hermitian potential is weak. Moreover, the level-attraction mechanism protects the zero modes from disorders. Except for the one-dimensional SSH model, we apply non-Hermitian potentials to the QWZ model and a second-order BHZ model according to the spatial distribution of edge states, where zero modes are recovered and robust against disorder. As we increase the strength of gain or loss, the edge state of the QWZ model shifts to one boundary despite disorder, and the corner state in the second-order BHZ model is gradually localizes at one corner. Our work reveals the level-attraction phenomenon of edge states in the non-Hermitian topological photonics. Furthermore, it provides a route to manipulate photonic topological states by gain and loss in topological photonic lattices beyond the SSH model. Beyond the models discussed here, our work suggests that the level-attraction mechanism could be a universal design principle for stabilizing edge states in a wide range of non-Hermitian systems, such as acoustic and mechanical systems.[60,61]

Acknowledgments. X.F. acknowledges partial support from Hong Kong RGC. This work was partly supported by the National Natural Science Foundation of China (Grant Nos. 12504562 and 12474218) and the HNNSF (Grant No. 2024JJ2061).

References

[1] Kittel C 2005 *Introduction to Solid State Physics* (John Wiley & Sons)
[2] Kubala B and König J 2002 *Phys. Rev. B* **65** 245301
[3] Bernier N R, Dalla Torre E G, and Demler E 2014 *Phys. Rev. Lett.* **113** 065303
[4] Bernier N R, Tóth L D, Feofanov A K, and Kippenberg T J 2018 *Phys. Rev. A* **98** 023841
[5] Grigoryan V L, Shen K, and Xia K 2018 *Phys. Rev. B* **98** 024406
[6] Harder M, Yang Y, Yao B M, Yu C H, Rao J W, Gui Y S, Stamps R L, and Hu C M 2018 *Phys. Rev. Lett.* **121** 137203
[7] Yu W, Wang J, Yuan H Y, and Xiao J 2019 *Phys. Rev. Lett.* **123** 227201
[8] Boventer I, Dör inger C, Wolz T, Macêdo R, Lebrun R, Kläui M, and Weides M 2020 *Phys. Rev. Research* **2** 013154
[9] Lu Q, Guo J, Zhang Y L, Fu Z, Chen L, Xiang Y, and Xie S 2023 *ACS Photonics* **10** 699
[10] Bleu O, Choo K, Levinsen J, and Parish M M 2024 *Phys. Rev. A* **109** 023707
[11] Gardin A, Bourcin G, Person C, Fumeaux C, Lebrun R, Boventer I, Tettamanzi G C, and Castel V 2025 *Phys. Rev. Appl.* **23** 014048
[12] Jiang B, Li Y Y, Liu J J, Wang C, and Jiang J H 2025 *Chin. Phys. Lett.* **42** 120403
[13] Heiss W D 2012 *J. Phys. A: Math. Theor.* **45** 444016
[14] Xu H, Mason D, Jiang L, and Harris J G E 2016 *Nature* **537** 80
[15] Mao W, Fu Z, Li Y, Li F, and Yang L 2024 *Sci. Adv.* **10** eadl5037
[16] Hodaei H, Hassan A U, Wittek S, Garcia-Gracia H, El-Ganainy R, Christodoulides D N, and Khajavikhan M 2017 *Nature* **548** 187
[17] Cao Y and Yan P 2019 *Phys. Rev. B* **99** 214415
[18] Kononchuk R, Cai J, Ellis F, Kottos T, and Alù A 2022 *Nature* **607** 697
[19] Lai Y H, Lu Y K, Suh M G, Yuan Z, and Vahala K 2019 *Nature* **576** 65
[20] Lin Z, Ramezani H, Eichelkraut T, Kottos T, Cao H, and Christodoulides D N 2011 *Phys. Rev. Lett.* **106** 213901
[21] Feng L, Xu Y L, Fegadolli W S, Lu M H, Oliveira J E B, Almeida V R, Chen Y F, and Scherer A 2013 *Nat. Mater.* **12** 108
[22] Huang Y, Verrier N, Burin A L, and Cao H 2017 *Nanophotonics* **6** 977
[23] He T, Zhang Z, Zhu J, Shi Y, Li Z, Wei H, Wei Z, Li Y, Wang Z, Qiu C W, and Cheng X 2023 *Light Sci. Appl.* **12** 229
[24] Wu M, Peng R, Liu J, Zhao Q, and Zhou J 2020 *Phys. Rev. Lett.* **125** 137703
[25] Song W, Sun W, Chen C, Song Q, Xiao S, Zhu S, and Li T 2019 *Phys. Rev. Lett.* **123** 165701
[26] Zhou B, Lu H Z, Chu R L, Shen S Q, and Niu Q 2008 *Phys. Rev. Lett.* **101** 246807

[27] Chen R, Chen C Z, Zhou B, and Xu D H 2019 *Phys. Rev. B* **99** 155431
[28] Bender C M and Boettcher S 1998 *Phys. Rev. Lett.* **80** 5243
[29] Chan C T 2025 *Phys. Rev. Lett.* **135** 080001
[30] Haldane F D M and Raghu S 2008 *Phys. Rev. Lett.* **100** 013904
[31] Raghu S and Haldane F D M 2008 *Phys. Rev. A* **78** 033834
[32] Wang Z, Chong Y D, Joannopoulos J D, and Soljačić M 2008 *Phys. Rev. Lett.* **100** 013905
[33] Wang Z, Chong Y, Joannopoulos J D, and Soljačić M 2009 *Nature* **461** 772
[34] Khanikaev A B, Mousavi S H, Tse W K, Kargarian M, MacDonald A H, and Shvets G 2013 *Nat. Mater.* **12** 233
[35] Chen W J, Jiang S J, Chen X D, Zhu B, Zhou L, Dong J W, and Chan C T 2014 *Nat. Commun.* **5** 5782
[36] Ma T and Shvets G 2016 *New J. Phys.* **18** 025012
[37] Chen X D, Zhao F L, Chen M, and Dong J W 2017 *Phys. Rev. B* **96** 020202
[38] Ye L, Yang Y, Hang Z H, Qiu C, and Liu Z 2017 *Appl. Phys. Lett.* **111** 251107
[39] He X T, Liang E T, Yuan J J, Qiu H Y, Chen X D, Zhao F L, and Dong J W 2019 *Nat. Commun.* **10** 872
[40] Xie B Y, Wang H F, Zhu X Y, Lu M H, Chen Z D, Jiang J H, Lu M H, and Chen Y F 2020 *Nat. Commun.* **11** 3768
[41] Takata K and Notomi M 2018 *Phys. Rev. Lett.* **121** 213902
[42] Hashemi A, Pereira E L, Li H, Lado J L, and Blanco-Redondo A 2025 *Nat. Mater.* **24** 1393
[43] Zhang K L, Wu H C, Jin L, and Song Z 2019 *Phys. Rev. B* **100** 045141
[44] Lu L, Fu L, Joannopoulos J D, and Soljačić M 2013 *Nat. Photonics* **7** 294
[45] Yuan L, Lin Q, Xiao M, and Fan S 2018 *Optica* **5** 1396
[46] Harari G, Bandres M A, Lumer Y, Rechtsman M C, Chong Y D, Khajavikhan M, Christodoulides D N, and Segev M 2018 *Science* **359** eaar4003
[47] Bandres M A, Wittek S, Harari G, Parto M, Ren J, Segev M, Christodoulides D N, and Khajavikhan M 2018 *Science* **359** eaar4005
[48] Hafezi M, Demler E A, Lukin M D, and Taylor J M 2011 *Nat. Phys.* **7** 907
[49] Chen J, Shi A, Peng Y, Peng P, and Liu J 2024 *Chin. Phys. Lett.* **41** 037103
[50] Barik S, Karasahin A, Flower C, Cai T, Miyake H, DeGottardi W, Hafezi M, and Waks E 2018 *Science* **359** 666
[51] Qi X L, Wu Y S, and Zhang S C 2006 *Phys. Rev. B* **74** 085308
[52] Schindler F, Cook A M, Vergniory M G, Wang Z, Parkin S S, Bernevig B A, and Neupert T 2018 *Sci. Adv.* **4** eaat0346
[53] Seshadri R, Dutta A, and Sen D 2019 *Phys. Rev. B* **100** 115403
[54] Asbóth J K, Oroszlány L, and Pályi A P 2016 *A Short Course on Topological Insulators: Band Structure and Edge States in One and Two Dimensions* volume 919 (Springer)
[55] Xu Z, Zhang R, Chen S, Fu L, and Zhang Y 2020 *Phys. Rev. A* **101** 013635
[56] Gao Z, Fryslie S T M, Thompson B J, Carney P S, and Choquette K D 2017 *Optica* **4** 323
[57] Wu L H and Hu X 2015 *Phys. Rev. Lett.* **114** 223901
[58] Mittal S, Orre V V, Leykam D, Chong Y D, and Hafezi M 2019 *Phys. Rev. Lett.* **123** 043201
[59] Song W, Wu S, Chen C, Chen Y, Huang C, Yuan L, Zhu S, and Li T 2023 *Phys. Rev. Lett.* **130** 043803
[60] Ma G, Xiao M, and Chan C T 2019 *Nat. Rev. Phys.* **1** 281
[61] Lu J, Deng W, Huang X, Ke M, and Liu Z 2025 *Adv. Mater.* **37** 2307998